Determination of Time-Dependent Inositol-1,4,5-Trisphosphate Concentrations during Calcium Release in a Smooth Muscle Cell

Charles C. Fink, Boris Slepchenko, and Leslie M. Loew
Department of Physiology and Center for Biomedical Imaging Technology, University of Connecticut Health Center, Farmington, Connecticut 06030

ABSTRACT The level of $[InsP_3]_{cyt}$ required for calcium release in A7r5 cells, a smooth muscle cell line, was determined by a new set of procedures using quantitative confocal microscopy to measure release of $InsP_3$ from cells microinjected with caged $InsP_3$. From these experiments, the $[InsP_3]_{cyt}$ required to evoke a half-maximal calcium response is 100 nM. Experiments with caged glycerophosphoryl-myo-inositol 4,5-bisphosphate ($GPIP_2$), a slowly metabolized analogue of $InsP_3$, gave a much slower recovery and a half-maximal response of an order of magnitude greater than $InsP_3$. Experimental data and highly constrained variables were used to construct a mathematical model of the $InsP_3$-dependent $[Ca^{2+}]_{cyt}$ changes; the resulting simulations show high fidelity to experiment. Among the elements considered in constructing this model were the mechanism of the $InsP_3$-receptor, $InsP_3$ degradation, calcium buffering in the cytosol, and refilling of the ER stores via sarcoplasmic endoplasmic reticulum ATPase (SERCA) pumps. The model predicts a time constant of 0.8 s for $InsP_3$ degradation and 13 s for $GPIP_2$. $InsP_3$ degradation was found to be a prerequisite for $[Ca^{2+}]_{cyt}$ recovery to baseline levels and is therefore critical to the pattern of the overall $[Ca^{2+}]_{cyt}$ signal. Analysis of the features of this model provides insights into the individual factors controlling the amplitude and shape of the $InsP_3$-mediated calcium signal.

INTRODUCTION

Inositol-1,4,5-trisphosphate ($InsP_3$)-mediated calcium release is an important intracellular signaling mechanism in many cell types (Berridge, 1993). How the amplitude and duration of an $[InsP_3]_{cyt}$ signal leads to a specific spatial and temporal $[Ca^{2+}]_{cyt}$ pattern has great bearing on many physiological functions. Heterogeneity in the molecules involved in $InsP_3$-mediated calcium release for different types of cells suggest that a good deal of specificity can be set at this level. Variability exists in the multiple isoforms of the $InsP_3$ receptor expressed from cell to cell (Wojcikiewicz, 1995; De Smedt et al., 1997); the isoforms have been shown to have different calcium release properties in response to $InsP_3$ and calcium (Bezprozvanny et al., 1991a; Hagar and Ehrlich, 1998; Ramos-Franco et al., 1998b; Ramos-Franco et al., 1998a). How these multiple isoforms function to carry out a specific signaling role within a cell is a topic under active investigation. $InsP_3$ degradation and production pathways vary among cell types (Glanville et al., 1989; Sims and Allbritton, 1998); these differences can allow cells to finely control their $[InsP_3]_{cyt}$ in response to a variety of stimuli (Dupont and Erneux, 1997). In addition, the amount of $InsP_3$ needed to evoke a calcium transient appears to be different from cell to cell. For example, Purkinje cells have been shown to require micromolar concentrations of $[InsP_3]_{cyt}$ to evoke calcium release, while other cell types have been shown to require more than an order of magnitude lower $[InsP_3]_{cyt}$ for the same size response (Khodakhah and Ogden, 1993; Ogden and Capiod, 1997). Clearly, cellular control over $[InsP_3]_{cyt}$ and $[Ca^{2+}]_{cyt}$ is finely regulated and is of great importance for the specificity of signal transduction from external stimuli.

However, the fundamental question of how much $InsP_3$ is required to initiate calcium release from the endoplasmic and sarcoplasmic reticular stores has been difficult to address. As of yet, there is no fluorescent indicator for $InsP_3$ as there is for calcium and other ions, so visualization of in vivo dynamics during a calcium release event is not possible. Despite this limitation, a variety of techniques have been introduced with the goal of ascertaining the relationship between $[InsP_3]_{cyt}$ and the characteristics of calcium signals. Much has been learned about cellular $[InsP_3]_{cyt}$ dynamics using in vitro experimental approaches. Competitive radioactive binding assays have been used to determine relative changes in $[InsP_3]_{cyt}$ during a signaling event (Wang et al., 1995; Burgess et al., 1985). Much has been learned about the biochemical and electrophysiological properties of $InsP_3$ receptors using lipid bilayer and microsomal preparations (Watras and Benevolensky, 1987; Bezprozvanny et al., 1991). A number of experimental techniques have been introduced with the goal of assaying $[InsP_3]_{cyt}$ in situ. Permeabilized cell preparations have been used to study the $InsP_3$-mediated release in a smooth muscle cell line (Missiaen et al., 1992, 1995, 1996) by assaying release of preloaded ^{45}Ca. An ingenious idea has been proposed (Luzzi et al., 1996) for using a cellular biosensor to measure dynamic $InsP_3$ concentration from nanoliter volumes of cytoplasm sampled by capillary electrophoresis. The introduction of caged $InsP_3$ (Walker et al., 1987; Walker et al., 1989), photolyzable upon exposure to uv light, has provided a powerful tool for introducing con-

Received for publication 6 January 1999 and in final form 9 April 1999.
Address reprint requests to Dr. Leslie M. Loew, Department of Physiology, University of Connecticut Health Center, 263 Farmington Avenue, Farmington, CT 06030. Tel.: 860-679-3568; Fax: 860-679-1269; E-mail: les@volt.uchc.edu.

0006-3495/99/07/617/12 $2.00

trolled quantities of $InsP_3$ into the cell with minimal disturbance of the intracellular environment. Assays for calibration of uncaging efficiency have been performed, typically substituting caged ATP for $InsP_3$ (Wootton et al., 1995) because of complications involved in directly assaying $InsP_3$. These calibrations are typically performed in a cuvette or microfilament. Dose-dependent calcium responses to $InsP_3$ exposure can be used to assay how $InsP_3$ regulation of calcium release occurs in an intact cell system (Khodakhah and Ogden, 1995; Oancea and Meyer, 1996).

In this paper, we determine the levels of $InsP_3$ required for calcium release in A7r5 cells, a well characterized cultured smooth muscle cell line from embryonic rat thoracic aorta (Kimes and Brandt, 1976). A7r5 cells have been used as a model for $InsP_3$-mediated calcium release from endoplasmic reticulum (ER) and sarcoplasmic reticulum (Missiaen et al., 1992; Sugiyama and Goldman, 1995; Missiaen et al., 1997) and have been shown to generate $InsP_3$-mediated calcium waves in response to hormonal stimulation (Blatter and Wier, 1992). A relatively simple method for accurately calibrating $InsP_3$ uncaging efficiency, based on quantitative confocal fluorescence microscopy (Fink et al., 1998), is introduced. The sensitivity of calcium release to $[InsP_3]_{cyt}$ is characterized by a half-maximal sensitivity in the range of 100 nM $InsP_3$. The dependence of calcium recovery on $InsP_3$ degradation has been investigated by determining the time course of cytosolic calcium levels following stimulus by $InsP_3$ and glycerophosphoryl-myo-inositol 4,5-bisphosphate ($GPIP_2$), a slowly hydrolyzable analogue of $InsP_3$. The $GPIP_2$ experiments indicate that the calcium uptake and extrusion processes cannot reduce $[Ca^{2+}]_{cyt}$ until $[InsP_3]_{cyt}$ is degraded. To derive the rates for $InsP_3$ production and degradation, the experimental results were simulated using Virtual Cell, a modeling tool developed in our laboratory (Schaff et al., 1997). By combining the experimental and modeling approaches, we can directly compare $[InsP_3]_{cyt}$ and $[Ca^{2+}]_{cyt}$ time courses after uncaging.

MATERIALS AND METHODS

Cell culture

A7r5 cells, a rat smooth muscle cell line from the thoracic aorta, were obtained from American Type Culture Collection (Manassas, VA). After thawing, cells were maintained in plastic petri dishes in Dulbecco's modified Eagle's medium with 4 mM L-glutamine adjusted to contain 1.5 g/L sodium bicarbonate, 4.5 g/L glucose, and a 1.0-mM solution of 90% sodium pyruvate and 10% fetal bovine serum. Cells were plated on coverslips and kept in a 5% CO_2 incubator at 37°C. When cells grew to confluence the coverslips were affixed to an open-welled plastic chamber, covered with Earle's balanced salt solution, and subsequently used for experimentation.

Microinjection and calcium imaging

Cells were microinjected with a solution containing 1–10 mM 1-(2-nitrophenyl)ethyl (NPE)-caged $InsP_3$ (Calbiochem, San Diego, CA) and 0.4–0.67 mM Calcium Green-1 conjugated to 10 kD Dextran (CG-1, Molecular Probes, Eugene, OR) in a solution containing 135 mM potassium, 10 mM aspartate, and 10 mM HEPES, buffered to pH 7.2. Later calculations showed that injections typically ranged from 3–5% of the cytosolic volume. Cells were imaged on an inverted Ziess LSM410 confocal microscope (Ziess, Thornwood, NY) after a 30-min recovery period. All experiments on the Ziess were performed at room temperature (22–24°C). A *z*-section through the soma was taken to quantify the concentration of CG-1; thus, the dilution of NPE-$InsP_3$ that occurred upon injection can also be calculated. A *z*-slice was selected with the soma in focus in the plane of maximal fluorescence intensity and initial CG-1 fluorescence was scanned at 488 nm with a 515- to 560-nm emission. For uncaging, the cell was subjected to a 364-nm scan, followed immediately by a time series of CG-1 fluorescence (excitation 488 nm, emission >515 nm) at 1-s intervals.

To determine the dilution factor for CG-1 (and therefore for NPE-$InsP_3$ or NPE-$GPIP_2$), calibration slides of CG-1 were scanned at the same confocal microscope settings as were used for the microinjected cell using the procedure detailed in Fink et al. (1998). These slides were prepared from various concentrations of CG-1 in a calcium buffer solution with approximately the same calcium concentration found in the A7 cells (64.5 nM); the dye was imaged between two coverslips with the same parameters used for the cellular CG-1 imaging. In order to check whether the cells had resting calcium levels near 64.5 nM, 10 cells were injected with equal concentrations of Texas Red-10 kD dextran and CG-1; dilution factors calculated from both dyes indicated that the cytosolic CG-1 was overestimated systematically by 6%. After this correction to all of the CG-1 dilution factors, a paired *t*-test gave a confidence level of 0.999987 for the correlation of the intracellular concentrations of Texas Red-10 kD dextran and CG-1.

Bleaching during the course of an uncaging series varied from almost negligible to about 25% of the initial CG-1 signal; each run was therefore individually corrected for the approximately linear dependence of bleaching on the duration of light exposure. The data are presented with this correction already included. To obviate the problem of accurate calibration of $[Ca^{2+}]_{cyt}$ with in vitro calibration solutions, calcium changes for uncaging experiments are expressed relative to the maximum change for a given cell (see below).

For some experiments, cells were imaged on an inverted NORAN confocal microscope; these experiments were performed at 37°C. CG-1 calcium imaging and concentration calibration was done as described above; however, because of the fast scanning capabilities of the NORAN, images were obtained at speeds up to 32/s. Another difference is that the uv source for uncaging is an arc lamp whose exposure length is controlled by a computer-controlled shutter, instead of the uv laser. The amount of $InsP_3$ released was a small percentage of the caged $InsP_3$ contained in the cells, and many calcium responses to repeated uv flashes could be obtained from a single cell.

After some experiments, calcium signals were recorded after addition of bradykinin (500 nM) to ascertain what calcium levels were produced by physiologically relevant levels of $InsP_3$. To determine fluorescence levels of CG-1 in saturating $[Ca^{2+}]_{cyt}$, 10 μM ionomycin was added after some experiments. In general, fluorescence changes following uncaging or bradykinin stimulation were well below values corresponding to saturating $[Ca^{2+}]_{cyt}$.

Uncaging efficiency calibration

The efficiency of uncaging was calibrated in our systems by assaying the production of protons with the uncaging of NPE-caged ATP (generously provided by Dr. Yale E. Goldman), which is known to uncage similarly to NPE-$InsP_3$ (Walker et al., 1989). Calibrations cannot be performed in this manner on NPE-$InsP_3$ itself because of the tendency of the phosphate groups to act as buffers. However, at pH > 6.5 and in the presence of magnesium, the phosphate groups in NPE-ATP and ATP do not act as buffers to the released protons. Solutions were prepared of 1 mM NPE-ATP, 10 mM MgCl, 100 mM KCl, 10 μM SNARF-1, and 0.5 to 10 mM Tris (pH 8.3) in double distilled water. Droplets of this solution small enough to fit inside the entire field of view used for uncaging were injected under paraffin oil onto a coverslip mounted to a plastic-welled chamber

identical to the one used for cellular experiments. Before and after uncaging of a droplet on the confocal microscope, SNARF-1 was ratio-imaged using an excitation wavelength of 488 nm and emission filters of 510–560 nm and ≥630 nm. Calibration slides were imaged under the same conditions; these slides were of the bubble solution (minus the NPE-ATP) with increasing amounts of added acid (HCl).

As a double check of this method, some experiments were performed in which quantum efficiency of uncaging was calculated directly on the NPE-$InsP_3$ by preparing a solution of 1 mM NPE-$InsP_3$ and 0.67 mM CG-1 in a solution containing 135 mM potassium, 10 mM aspartate, and 10 mM HEPES, buffered to pH 7.2. Bubbles of this solution were placed on a coverslip immersed in paraffin oil as described above; wax was used to create a well of even smaller volume (<50 μl), which facilitated extraction. After uncaging, a *z*-series of the CG-1 fluorescence was obtained and the volume of the bubble was calculated using VoxelView software (Vital Images, Minneapolis, MN) on Silicon Graphics (Mountain View, CA) workstations. The $InsP_3$ that was uncaged was calculated using competitive radioligand binding assay (Benevolensky et al., 1994).

Mathematical modeling

The calcium response to uncaging $InsP_3$ (or $GPIP_2$) and its time course during the subsequent degradation of $InsP_3$ were modeled using Virtual Cell software (Schaff et al., 1997). Calcium release from the ER within the overall model is based on the 8-state model for the $InsP_3$ receptor originally proposed by DeYoung and Keizer (1992); in addition to the requirement for $InsP_3$ binding to open the calcium channel, it includes separate calcium-dependent activation and inactivation processes. As the channel becomes inhibited, $[Ca^{2+}]_{cyt}$ is restored to resting levels via action of the SERCA pump and calcium buffers. Thus, the calcium dynamics is governed by the ordinary differential equation (Sneyd et al., 1995),

$$\frac{\partial[\mathrm{Ca}]}{\partial t} = \beta(J_{\mathrm{channel}} - J_{\mathrm{pump}} + J_{\mathrm{leak}}) \tag{1}$$

where $J_{channel}$, J_{pump}, and J_{leak} are the rates of the calcium concentration change due to the channel release, pump uptake, and leak, respectively. The factor β describes calcium buffering (Wagner and Keizer, 1994).

We use the simplified version (Li and Rinzel, 1994) of the model proposed by De Young and Keizer (1992) to describe the calcium release through an $InsP_3$-sensitive channel. In this model,

$$J_{\mathrm{channel}} = J_{\max}\left(\left(\frac{[I]}{[I]+K_{\mathrm{I}}}\right)\left(\frac{[\mathrm{Ca}]}{[\mathrm{Ca}]+K_{\mathrm{act}}}\right)h\right)^3\left(1-\frac{[\mathrm{Ca}]}{[\mathrm{Ca\_ER}]}\right) \tag{2}$$

where J_{max} is the maximal possible rate; $[I]$ stands for the concentration of $InsP_3$ (or $GPIP_2$), and $[I] = ([I]_{unc})\exp(-t/\tau) + [I]_0$, where $[I]_{unc}$ is the uncaged concentration, $[I]_0$ is the steady state concentration, t is the time following uncaging, τ is the time constant for $InsP_3$ degradation; K_I is the dissociation constant for $InsP_3$ ($GPIP_2$) binding to a channel; K_{act} is the dissociation constant for calcium binding to an activation site; [Ca_ER] is the calcium concentration in ER; and h is the probability that Ca^{2+} occupies its inhibitory binding site. The governing equation for h is

$$\frac{\partial h}{\partial t} = k_{\mathrm{on}}(K_{\mathrm{inh}} - ([\mathrm{Ca}] + K_{\mathrm{inh}})h) \tag{3}$$

where k_{on} is the on-rate of calcium binding to the inhibitory site and K_{inh} is the corresponding dissociation constant.

We describe the sarcoplasmic endoplasmic reticulum ATPase pump uptake by a Hill-type equation (Lytton et al., 1992; Sneyd et al., 1995),

$$J_{\mathrm{pump}} = V_{\max}\frac{[\mathrm{Ca}]^2}{[\mathrm{Ca}]^2 + K_{\mathrm{p}}^2} \tag{4}$$

where V_{max} is the maximal rate and K_p is the corresponding dissociation constant.

Fast calcium buffering is described within the steady state approximation by the expression (Wagner and Keizer, 1994)

$$\beta = \left(1 + \frac{[B]_{\mathrm{end}}}{K_{\mathrm{end}}} + \frac{[B]_{\mathrm{ex}}K_{\mathrm{ex}}}{([\mathrm{Ca}]_{\mathrm{ex}} + K_{\mathrm{ex}})^2}\right)^{-1} \tag{5}$$

where $[B]_{end}$, K_{end}, $[B]_{ex}$, and K_{ex} stand for the concentrations and dissociation constants of endogenous and exogenous buffers. Finally,

$$J_{\mathrm{leak}} = L\left(1 - \frac{[\mathrm{Ca}]}{[\mathrm{Ca\_ER}]}\right) \tag{6}$$

where the leak constant L is to be determined from the condition of a steady-state flux balance. The system of ordinary differential equations, Eqs. 1 and 3, with the initial conditions

$$[\mathrm{Ca}]_0 = 0.05\ \mu\mathrm{M}$$

$$h_0 = \frac{K_{\mathrm{inh}}}{[\mathrm{Ca}]_0 + K_{\mathrm{inh}}}$$

$$\text{and} \quad [I](t=0) = [I]_{\mathrm{unc}} + [I]_0$$

were integrated numerically by the Euler forward method with a time step of 1 ms.

Parameter values used in the simulations are given in Table 1. They are constrained by the published experimental data, experimental results obtained in the present work, and the steady state stability requirement, which reduces to the system of inequalities:

$$L > 0$$

and

$$\frac{d(J_{\mathrm{channel}} - J_{\mathrm{pump}} + J_{\mathrm{leak}})}{d[\mathrm{Ca}]} < 0.$$

TABLE 1 Parameter values for uncaging $InsP_3$

Parameter	Value	References
J_{max}	2880 μM s^{-1}	Bezprozvanny et al., 1991; Kupferman et al., 1997
K_{act}	0.17 μM	Constrained by stability conditions
K_{inh}	0.1 μM	Constrained by stability conditions
k_{on}	8.0 μM^{-1} s^{-1}	Fit to experiment
[Ca_ER]	400 μM	Miyawaki et al., 1997; Meldolesi and Pozzan, 1998
$[Ca]_0$	0.05 μM	Estimated from indicator fluorescence
$[I]_0$	0.01 μM	Present work and Missiaen et al., 1996
$[I]_{unc}$	0.858 μM	Experimentally determined
K_I	0.03 μM	Fit to experiment
V_{max}	5.85 μM s^{-1}	Gill and Chueh, 1985; Lytton et al., 1992
K_p	0.24 μM	Gill and Chueh, 1985; Lytton et al., 1992
$[B]_{end}/K_{end}$	40	Xu et al., 1997
$[B]_{ex}$	11.35 μM	Measured $[CG\text{-}1]_{cyt}$
K_{ex}	0.26 μM	Eberhard and Erne, 1991
L	0.0804 μM s^{-1}	Determined by the steady state balance condition

Thus, the values for J_{max}, V_{max}, K_p, $[I]_0$, and binding ratio for endogenous buffers are estimated from the published experimental data. The values of K_{act} and K_{inh} are bounded by the requirement of a steady state stability on one hand and by the delay between the light flash and the maximum calcium response (<1 s under conditions of saturated response) on the other. The experimentally determined concentration and the published (Eberhard and Erne, 1991) dissociation constant of the fluorescent indicator Calcium Green-1 were used for $[B]_{ex}$ and K_{ex} of the high-affinity exogenous buffer. The k_{on} value is constrained by the actual maximal calcium concentrations under the saturation conditions, which were estimated to be in the range of 0.5–0.7 μM.

The determination of the final set of parameters was substantially facilitated by sensitivity analysis, a component of the Virtual Cell system. We determined which parameters were most responsible for controlling the key features of the calcium response: the lag time, the maximum amplitude, and the time course of the recovery phase. The logarithmic sensitivities ($\partial \log[\mathrm{Ca}]/\partial \log\alpha$), α is a parameter) for the parameter set, used for the simulation of a calcium response to a $InsP_3$ uncaging, are presented in Table 2.

To compare simulation results with the experimental data, we first translated the normalized fluorescence response $f = (F - F_{min})/F_{max} - F_{min})$, where F, F_{max}, and F_{min} are the current fluorescence, maximal fluorescence following a saturating level of uncaged $InsP_3$, and baseline fluorescent intensity, respectively, into a relative calcium response

$$\frac{[\mathrm{Ca}] - [\mathrm{Ca}]_{min}}{[\mathrm{Ca}]_{max} - [\mathrm{Ca}]_{min}} = f\frac{F_\infty - F_{max}}{F_\infty - fF_{max} - (1-f)F_{min}}, \quad (7)$$

where F_∞ is the fluorescent intensity at a saturating calcium concentration experimentally determined following addition of 10 μM ionomycin. Eq. 7 can be directly derived from the standard equation for calculating $[Ca^{2+}]$ from a single wavelength indicator (Grynkiewicz et al., 1985),

$$[\mathrm{Ca}] = K_{CG}\frac{F - F_0}{F_\infty - F}$$

where K_{CG} is the Calcium Green dissociation constant and F_0 is the fluorescent intensity at a zero calcium concentration level. Because Eq. 7 represents a ratio of differences, both F_0 and K_{CG} drop out. Thus, using the dimensionless relative change in $[Ca^{2+}]_{cyt}$ as expressed in Eq. 7, obviates the problem of accurate in vivo calibration of the $[Ca^{2+}]_{cyt}$ in each experiment and permits us to relate the modeling results to an accurately determined experimental variable.

TABLE 2 Sensitivity Analysis

Parameter	t = 0.25 s	t = 0.75 s	t = 7.0 s
V_{max}	−0.0228	−0.0644	−1.2674
J_{max}	1.8604	0.9096	0.8579
$[I]_0$	−0.0350	−0.0062	−0.0193
$[I]_{unc}$	0.2207	0.1452	0.2147
K_I	−0.1857	−0.1390	−0.1955
K_{act}	−3.8125	−0.9980	−0.7723
K_{inh}	0.2438	0.4455	0.7736
K_p	0.0377	0.0209	0.5587
k_{on}	−0.0819	−0.7291	−0.6711
$[B]_{ex}$	−0.7061	−0.1623	0.0361
K_{ex}	0.3833	0.0180	0.0320
$[B]_{end}/K_{end}$	−1.1038	−0.6662	0.3643
τ	0.0353	0.0711	0.3477

Logarithmic sensitivities, $\partial\log[\mathrm{Ca}]/\partial\log\alpha$, for uncaging 0.86 μM $InsP_3$.

RESULTS

$InsP_3$ uncaging efficiency

Establishing the concentration of $InsP_3$ that is uncaged in the cell when subjected to a measured uv flash is a two-step process: first, the concentration of caged molecules must be measured in the cell, and second, the fraction of caged molecules uncaged with a uv flash of known intensity must be determined.

In previous work (e.g., Khodakhah and Ogden, 1993), the whole cell patch configuration was employed to introduce a known concentration of $InsP_3$ within a single cell. We wished to microinject many cells on a coverslip in order to facilitate the collection of statistically significant data and to minimize perturbation of the intracellular milieu. Accordingly, we devised a new method for determining the intracellular concentration of the injected caged $InsP_3$. In order to calculate the concentration of caged $InsP_3$ inside the cell, the concentration of coinjected Calcium Green-1-dextran is determined. Because the concentrations of both molecules are known in the injection pipette, the dilution factor for the cell multiplied by the initial caged $InsP_3$ concentration in the microinjection pipette will give the final concentration of caged $InsP_3$ inside the cell. The concentration of a fluorescent dye can be calculated by a method outlined in an earlier paper (Fink et al., 1998). Briefly, before an uncaging flash, a confocal image with narrow pinhole settings is acquired within a central plane of the soma where the intensity is maximal; this intensity level should not vary over several microns along the optical axis. Our earlier work demonstrates that the fluorescence intensity measured in the center of such a slice is not diluted by contributions from planes outside the cell. Thus, the intensity measured under these conditions represents the true intensity of fluorescence inside the cell. Under the same microscope settings used to collect these confocal images, a series of slides made up with calibration solutions of varying concentrations of Calcium Green-1-dextran were imaged in order to determine the relationship between concentration of dye and measured fluorescence intensity. The dye slides were composed of varying concentrations of Calcium Green-1 in a solution of the approximate ionic strength, pH, and resting calcium concentration found inside the A7 cells (64.5 nM calcium, 100 mM KCl, 10 mM MOPS, pH 7.2). The dye slides were imaged in a plane at least 5 μm above the coverslip; the relationship between fluorescence intensity and dye concentration could be fitted to a straight line (Fig. 1 *a*). The resulting linear calibration can now be used with each cellular image in order to calculate the concentration of Calcium Green-1 inside the cell. Cells showed similar dilution factors, typically ranging from 3–5% of the cytosolic volume (3.3% ± 0.3%). Multiplying this dilution factor by the concentration of caged $InsP_3$ in the pipette yields the concentration of caged $InsP_3$ in the cytosol. To check this approach, especially the assumption that 64.5 nM is close to the resting calcium level, experiments were performed in

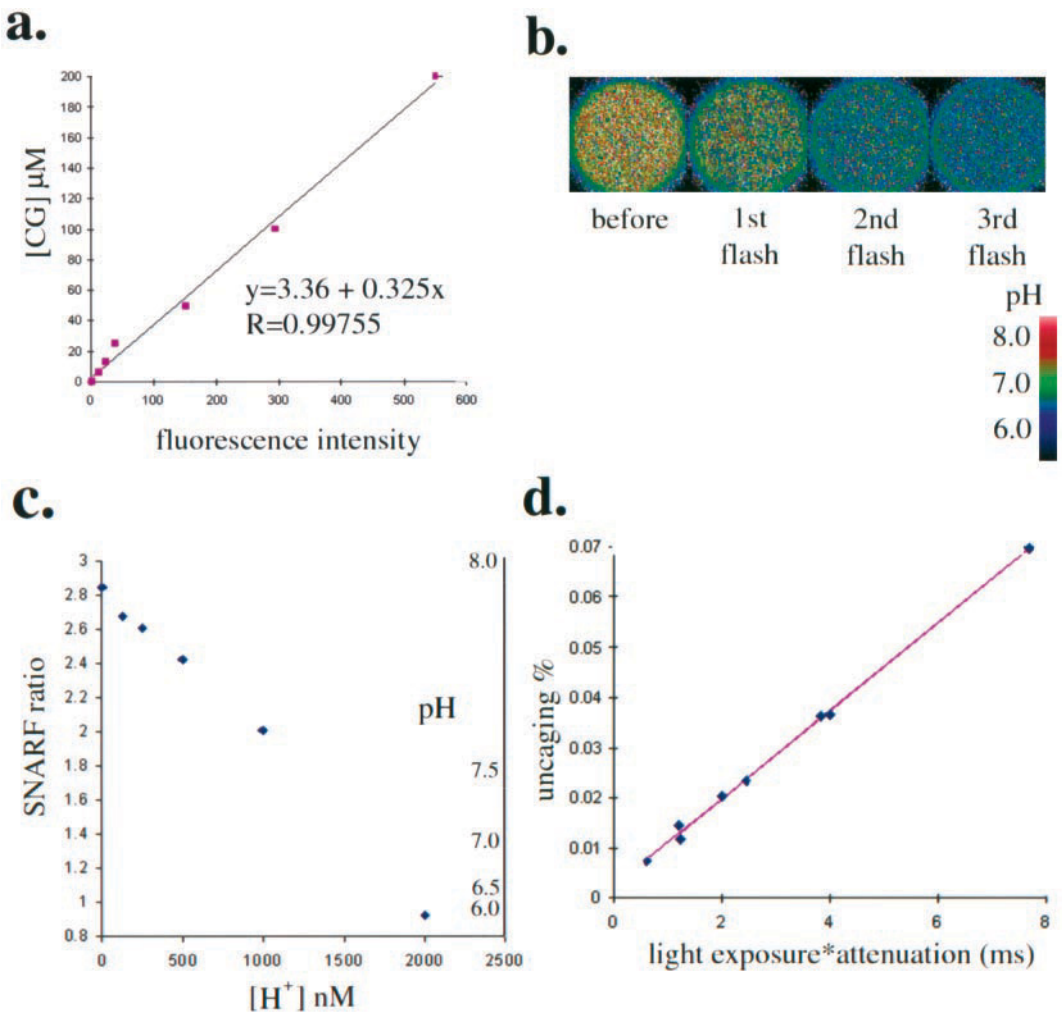

FIGURE 1 Quantitative calibration of uncaging. (*a*) Calibration plot of [CG-1] versus fluorescence intensity. A series of dye slides of increasing concentrations of CG-1 in 64.5 nM of calcium solution were imaged on the confocal microscope under identical settings. A straight line, intersecting near zero, was fitted with the equation $y = 3.36 + 0.325x$ ($R = 0.99755$). This equation was then used to calculate $[CG\text{-}1]_{cyt}$ for microinjected cells imaged under the same conditions. (*b*) An example of the calibrations performed on an aqueous droplet under paraffin oil. The droplet contains SNARF, a dual-emission pH indicator dye, NPE-ATP, and a Tris buffer. When flashed with uv light, a proton is released for each molecule of ATP uncaged; this can be measured by the drop in pH. (*c*) The pH indicator is calibrated by imaging another series of dye slides. The slides contain solutions of the Tris buffer used for the aqueous droplet experiments, SNARF, and increasing $[H^+]$ (HCl). By ratio imaging the dye slides, a linear calibration curve can be determined for SNARF ratio (or, alternatively, pH) versus $[H^+]$. (*d*) The relationship between uncaging percentage and light dosage was found to be linear, with an intersect near zero. An average of 0.0091% uncaging was seen to occur for 1 ms of unattenuated uv light exposure.

which cells were injected with Texas Red-10 kD dextran along with an equal concentration of CG-1. As discussed in the Methods section, cytosolic [CG-1] was found in this way to have a systematic overestimate of 6% and this correction was applied to the cytosolic concentrations of both CG-1 and caged $InsP_3$. This slight overestimate is most likely reflective of a somewhat higher average baseline $[Ca^{2+}]_{cyt}$ than the 64.5 nM chosen for our reference solution.

Next, the fraction of caged compound uncaged with a uv flash of a given light intensity needs to be determined. Efficiency of uncaging can be calibrated by taking advantage of the fact that for each molecule uncaged, a proton is released (Walker et al., 1988). A fluorescent pH indicator, such as SNARF, can be used to monitor pH change and the number of caged molecules uncaged could be back-calculated. Unfortunately, caged $InsP_3$ can't be calibrated by this method, since $InsP_3$ itself will act as a buffer throughout the effective pH range of SNARF, the pH indicator. Therefore, caged ATP is used; NPE-ATP has been shown to have a similar uncaging efficiency to NPE-$InsP_3$, and when in the presence of excess magnesium, does not act as a proton buffer above pH 6.5 (Walker et al., 1988). We wanted to be able to measure the proton formation under conditions as similar as possible to the physiological experiments. To do this, cell-sized droplets of aqueous solution were placed on the surface of a coverslip affixed to the same open-welled plastic chamber used for cells. The chamber was filled with paraffin oil so that the droplets would stay affixed to the coverslip on the inverted microscope. The droplets con-

tained 1 mM NPE-ATP, 10 mM MgCl, 100 mM KCl, 10 μM SNARF-1, and 0.5–10 mM Tris (pH 8.3) in d/d water; the concentration of Tris buffer was varied in order to assay increasingly sensitive (lower uncaging efficiency) events. SNARF is a dual emission ratiometric indicator; it is excited at the laser line 488 nm and a ratio is formed from emissions 510–560 nm and >630 nm. With increasing numbers of protons (lower pH) fluorescence from the >630 nm emission will decrease from the >630 nm emission and increase from the 510–560 nm emission. To be accurate, measurements made with SNARF should be obtained with physiological ranges (pH 7.0–8.0). Examples of the fluorescence changes in the aqueous droplets, displayed here as red/green emission ratios, are shown in Fig. 1 *b*. Ratio changes are converted to $[H^+]$ via calibration with solutions titrated with increasing concentrations of HCl in the same solution used for the aqueous bubbles, minus the caged ATP (Fig. 1 *c*). With each uncaging event, the change in $[H^+]$ divided by the concentration of caged ATP gives fraction of uncaging of that particular uv light dosage. The relationship between proton release and the intensity of the light flash is linear; this is illustrated in Fig. 1 *d* for the Zeiss LSM410. A separate calibration was performed when doing experiments on the NORAN confocal microscope (with a Xe arc lamp as the uv light source).

A check on the validity of these numbers was obtained by doing a limited number of direct calibration experiments on caged $InsP_3$ itself. In these experiments, a droplet of aqueous solution containing caged $InsP_3$ was placed on the surface of a coverslip, as was done for the NPE-ATP calibrations. A well of less than 50 μl was constructed from wax in order to facilitate the separation of the aqueous liquid from the oil. After uncaging with a specific uv flash intensity, the aqueous bubble was extracted from the oil and $InsP_3$ binding assays were performed. This provided the total mass of $InsP_3$ in the droplet; to obtain concentrations, this value is divided by the volume of the droplet, which was estimated by creating a three-dimensional reconstruction through multiple *z*-sections. Equivalent uncaging efficiencies were calculated by the two calibration methods.

Calcium responses from uncaged inositol phosphates ($InsP_3$ and $GPIP_2$)

When a caged $InsP_3$-loaded cell is uniformly exposed to a uv flash, a uniform calcium increase is observed within 0.5 s, followed by a gradual recovery of calcium levels. Fig. 2 *a* shows an example of such a collection of images; in this particular instance, the cell is subjected to a 250-ms flash which uncages 3.4 μM of $InsP_3$. The time course of the calcium response can be seen more clearly in a calcium-versus-time plot (Fig. 2 *b*). At room temperature, complete recovery is typically seen within 20 s. As long as the amount of $InsP_3$ released was a small fraction of the total amount injected, many responses can be obtained from the same cell.

Some experiments were performed with caged $GPIP_2$, a poorly metabolized analogue of $InsP_3$. $GPIP_2$ is reported to be 10–200 times more slowly degraded than InsP3 in various cell types (Bird et al., 1992). The amount of $GPIP_2$ uncaged in this example (Fig. 2 *b*) is somewhat higher (9.6 μM) than the amount of $InsP_3$ uncaged. In general the amount of $GPIP_2$ required to evoke a given calcium response was higher, consistent with its known lower effectiveness compared to $InsP_3$ in initiating calcium release (Bird et al., 1992). Although the rise to peak calcium levels is similar for both $GPIP_2$ and $InsP_3$, the recovery time is greatly prolonged for $GPIP_2$ (Fig. 2 *b*), requiring >30 s to return to baseline. With $GPIP_2$, it is usually not possible to evoke repetitive responses within the same cell, although a second and sometimes a third response can be evoked if sufficient time is allowed between uv flashes. This suggests that the long-lived calcium responses following $GPIP_2$ may desensitize the channel and/or deplete the stores. The fact that the $GPIP_2$-induced calcium signal decays more slowly than the signal following $InsP_3$ uncaging, suggests that the relaxation of $[Ca^{2+}]_{cyt}$ back to baseline levels must be preceded by the decay of $InsP_3$ (or $GPIP_2$).

Measurement of physiological $InsP_3$ response and check for indicator saturation

In order to check that the $InsP_3$-induced calcium release is physiologically relevant in this system, some experiments were performed in which an agonist stimulates $InsP_3$ production. Bradykinin is a nonapeptide that stimulates $InsP_3$ production in many cell types (Hall, 1992; Regoli et al., 1994), which ultimately results in a transient calcium elevation. Here, bradykinin was added to the bath at concentrations (500 nM) corresponding to a saturating dose in other cell types. Response versus time is shown for a sample cell in Fig. 2 *b*; after a short latency following agonist application, calcium levels can be seen to increase and subsequently return to baseline in 30 s. The calcium changes are consistent with the magnitude of the response seen in the uncaging experiments, suggesting that the $InsP_3$ production in response to bradykinin stimulus is at least as high as the threshold values calculated in the uncaging experiments. Application of a calcium ionophore, 10 μM ionomycin, to saturate the calcium green indicator gave still higher fluorescence and allowed us to perform a calibration of the calcium concentrations during uncaging and bradykinin stimulation (see methods and Fink et al., 1998).

Measurement of the sensitivity of calcium release to $InsP_3$

Experiments were done at 37°C on the NORAN confocal microscope, with incremental steps in flash exposure and light intensity. Fig. 3 *a* shows the calcium response from a typical experiment; the data were recorded at 8 images/s, and the concentration of $InsP_3$ uncaged with each flash is

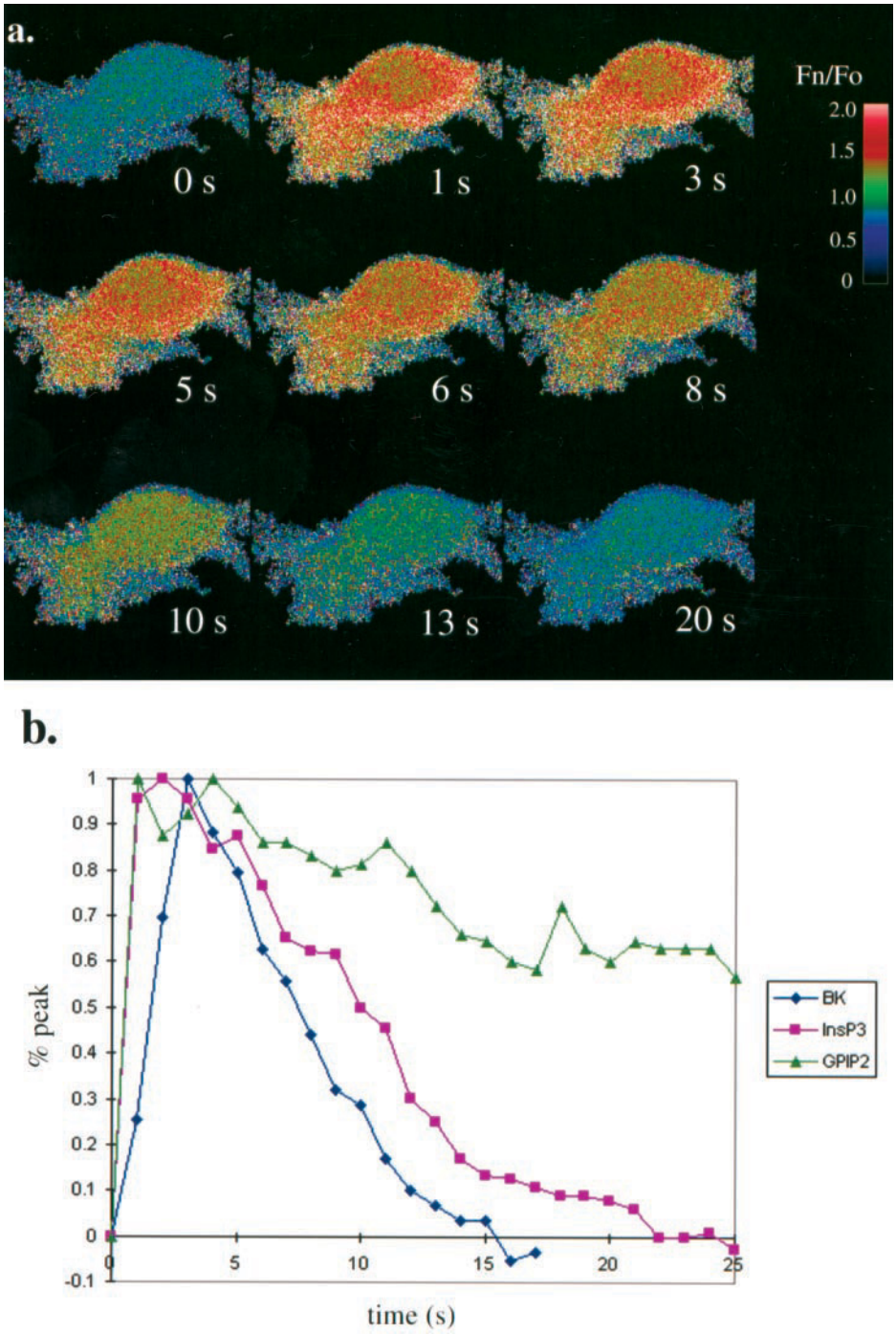

FIGURE 2 $[Ca^{2+}]_{cyt}$ responses in A7r5 cells following $InsP_3$ or $GPIP_2$ stimulation. (*a*) A typical experiment in which CG-1 fluorescence is imaged after uncaging of 3.4 μM $InsP_3$ by a uv flash at time 0 s. Images are shown as ratios of F_n over F_0. This experiment was performed at 22°C on the Ziess confocal microscope. (*b*) Time courses of various calcium responses elicited in A7r5 cells, expressed in terms of percentage peak of the CG-1 fluorescence. Examples are shown for three conditions: $InsP_3$ uncaging (*squares*), $GPIP_2$ uncaging (*triangles*), and exposure of the cells to 500 nM bradykinin in the medium (*diamonds*). Each cell was imaged as illustrated in (*a*), a region of interest was selected in the cell body, and normalized CG-1 fluorescence changes were plotted against time. The cell shown in (*a*) was used for the $InsP_3$ trace; for the $GPIP_2$ experiment, the amount of $GPIP_2$ uncaged was estimated to be 9.6 μM. All three experiments were performed at 22°C on the Ziess confocal microscope.

indicated. The data from this experiment is shown in graphical form in Fig. 3 *b*, *y*-axis values are the relative change in $[Ca^{2+}]_{cyt}$ following a uv flash, normalized so that the maximum change is 1.0. To establish an empirical dose-response relationship, the data is fit with a line in the form of the Hill equation:

$$y = (x^n/(k^n + x^n))$$

where y is the change in calcium green fluorescence intensity normalized to 1.0 at the maximum, x is the concentration of $InsP_3$ uncaged (in μM), k is the concentration of $InsP_3$ needed to elicit a half-maximal calcium response (EC_{50}), and n is the Hill coefficient (a value that indicates the apparent cooperativity of $InsP_3$ binding to its receptor in this reaction). For this cell, k is 73.8 nM and n is 1.8. This analysis was done for each cell and mean values ($\pm$ SE) were obtained for k (0.099 $\pm$ 0.023 μM) and n (2.50 $\pm$ 0.41) (analyses of 10 cells).

By way of comparison, some experiments were done with uncaging $GPIP_2$. As noted above, at most three uncaging events per cell were possible with $GPIP_2$, so it was not possible to determine k for individual cells. When single

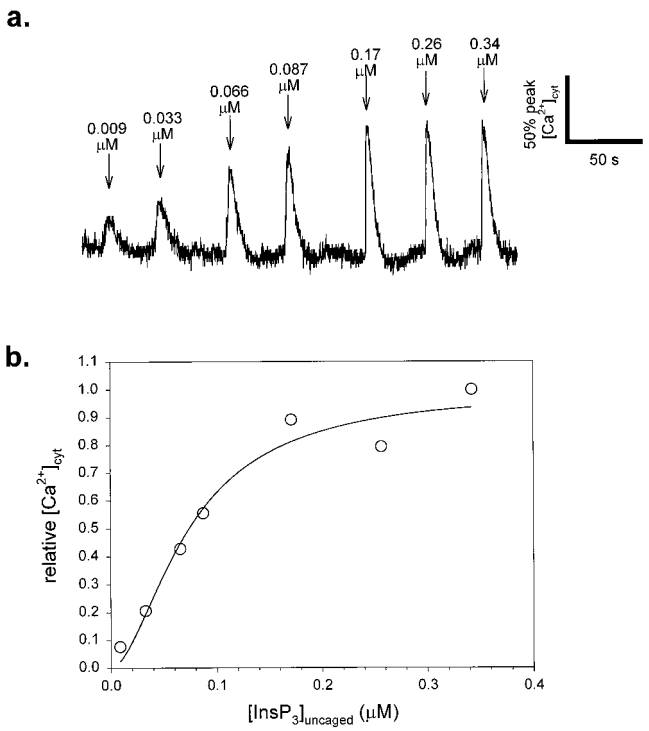

FIGURE 3 Titration of calcium release with varying concentrations of caged $InsP_3$ in a single cell. (*a*) Dose-response experiment on a single A7r5 cell, microinjected with CG-1 and NPE-InsP3. The CG-1 fluorescence was monitored over time while the cell was exposed to a series of increasing uv light dosages. The amount of $InsP_3$ uncaged with each flash is shown above the trace. This experiment was performed at 37°C on the NORAN confocal. (*b*) Measured dose-response of $[Ca^{2+}]_{cyt}$ to $[InsP_3]_{cyt}$ from the example in (*a*) is plotted. For each flash, the percent increase of calcium was calculated from Eq. 7. These increases were normalized to 1 within the experiment to the maximum increase observed, and plotted against $[InsP_3]$ uncaged (*open circles*). The data was fit (fitted curve is shown as black trace) with a high correlation ($R > 0.98$) to the Hill equation: $y = x^n/(k^n+x^n)$; where k is the concentration of $InsP_3$ needed to elicit a half-maximal calcium response (EC_{50}), and n is the Hill coefficient, a value which indicates the apparent cooperativity of $InsP_3$ binding to the receptor in this reaction. For this cell, $k = 73.8$ nM and $n = 1.8$.

experiments on a large number of cells ($n = 61$) are fitted to the Hill equation, an EC_{50} value of 1.228 ± 0.476 μM was obtained. This indicates that the $InsP_3R$ is approximately 10-fold more sensitive to $InsP_3$ than to $GPIP_2$. It should be noted that the Hill equation is used here as a phenomenological equation that permits us to compare the sensitivity of the $InsP_3R$ to $InsP_3$ in our cells to other preparations and also to permit comparison of its sensitivity to $InsP_3$ vs. $GPIP_2$. Thus k should not be confused with the dissociation constant (K_I in Table 1) for $InsP_3$ binding to its receptor. The fit of the experimental data to a mechanistic model for the calcium dynamics following uncaging will be explored in the next section.

Analysis of calcium dynamics

In order to gain a more detailed understanding of the $InsP_3$ dependence of the calcium signal in the A7r5 cells, we performed simulations based on a limited model of the process. The model was based on the interaction of four components: 1) calcium release through the $InsP_3$-dependent ER channel, 2) calcium uptake into the ER via the SERCA pump, 3) calcium buffering by both endogenous and exogenous (i.e., the calcium indicator) buffer, and 4) $InsP_3$ degradation. In addition, a small steady-state calcium permeability is assigned to the ER membrane to maintain the resting calcium level. Calcium extrusion or entry through the plasma membrane and calcium release through the ryanodine receptor are assumed to be of minor importance for the time scale of our experiment. The most important component is the $InsP_3$ receptor that forms the calcium channel; it consists of four subunits, each of which contains an $InsP_3$ binding site as well as two binding sites for calcium that, respectively, activate and inhibit opening of the calcium channel (Bezprozvanny et al., 1991a; De Young and Keizer, 1992). The details of this kinetic model and those associated with the other three components of the overall model are given in the Methods section and in Table 1.

Fig. 4 *a* shows averaged calcium recovery curves following stimulus with uncaged $InsP_3$ or $GPIP_2$; each data point is the mean of 10 experiments, and has been normalized within each cell to 1. Each of the 10 uncaging events chosen for Fig. 4 *a* has a calcium response approaching the maximum with an average concentration of uncaged $InsP_3$ of 0.86 μM, i.e., well above the EC_{50}. Also in this figure is the corresponding fit derived from the mathematical modeling for the same conditions. Using the set of parameters from Table 1, we obtained the best fit for the average calcium response to the $InsP_3$ uncaging with $K_I = 0.03$ μM and the $InsP_3$ degradation time $\tau = 0.8$ s. Using the same set of parameters we were able to fit the experiment on the $GPIP_2$ induced calcium release with $K_I = 0.11$ μM and a degradation time $\tau = 13.0$ s. This supports the idea that $InsP_3$ and $GPIP_2$ operate on the $InsP_3$ receptor channel via the same molecular mechanism. This is a prerequisite for the hypothesis, based on the different time courses for $InsP_3$ and $GPIP_2$, that calcium recovery must be preceded by the degradation of $InsP_3$. To facilitate this comparison, we have also included the results of the simulation for the $InsP_3$ and $GPIP_2$ degradation in Fig. 4 *a*. As can be seen, $InsP_3$ ($GPIP_2$) degrades at a significantly faster rate than the recovery of $[Ca^{2+}]_{cyt}$.

We are able to simulate the titration curve (Fig. 4 *b*), for the dependence of $[Ca]_{max}$ on the amount of uncaged $InsP_3$ for a typical single cell with the same model. As opposed to the empirical fit in Fig. 3 to a generic Hill equation, in Fig. 4 *b* the data is fit to our four-component model; small adjustments to some of the average parameters in Table 1 were necessary to account for cell-to-cell variations and the particular CG-1 level measured in this cell (15 μM). The theoretical curve is in good agreement with the experimental data for this typical cell. The same model and set of parameters could then be used to fit the full time courses of the $[Ca^{2+}]_{cyt}$ changes in the same cell following varying levels of $InsP_3$ uncaging as shown in Fig. 4 *c*; for this

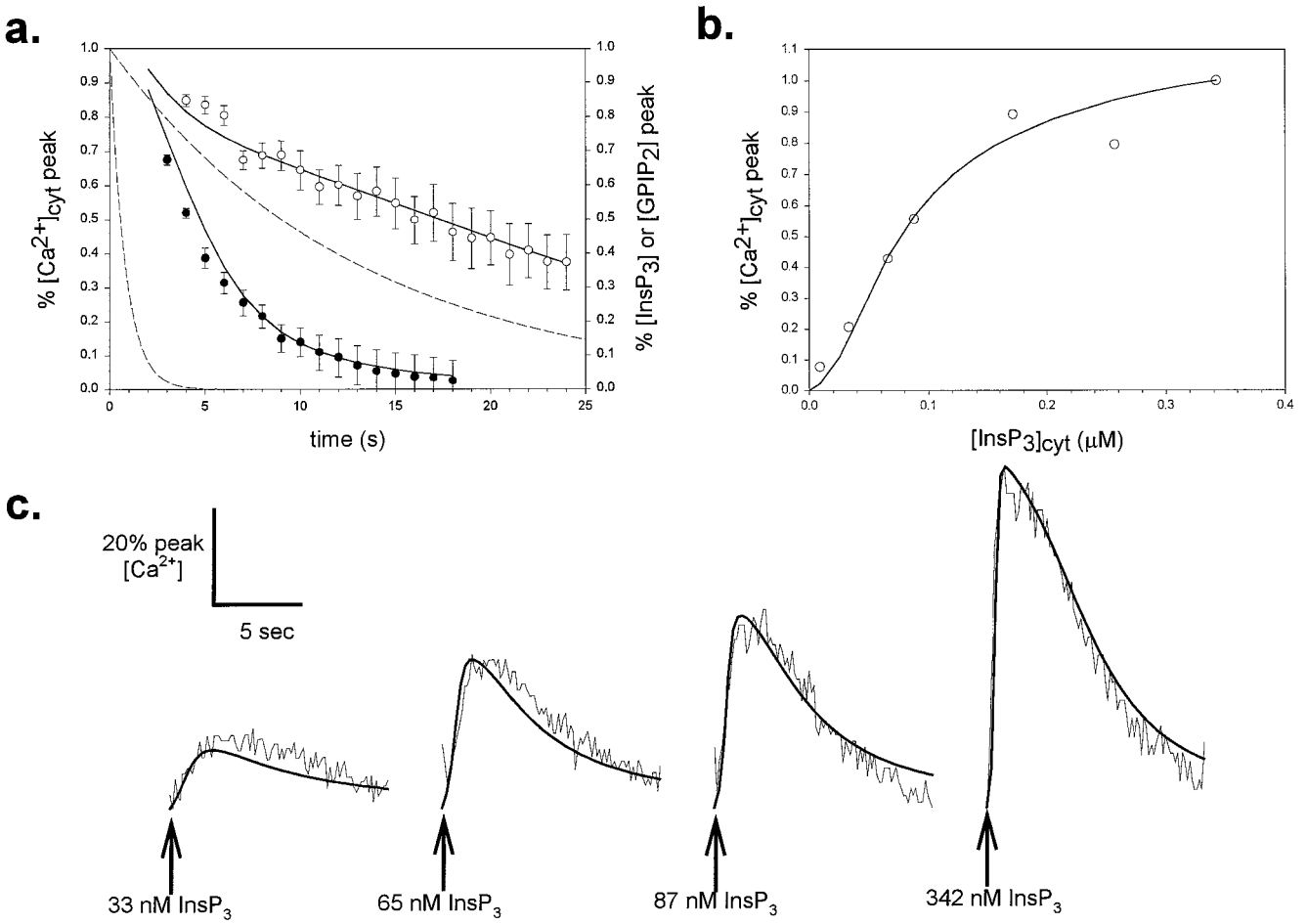

FIGURE 4 Mathematical modeling of $InsP_3$-induced calcium dynamics in A7r5 cells. (*a*) The time course of calcium levels following uncaging of either $InsP_3$ (*closed circles*) or $GPIP_2$ (*open circles*); each point represents the average of 10 experiments, each of which is normalized internally to 1.0 for the peak calcium concentration. These experiments were performed at 37°C on the NORAN confocal microscope; the average concentrations of metabolite uncaged is 0.858 μM $InsP_3$ and 0.52 μM $GPIP_2$. The fitted lines are the calculated values for the time course of $[Ca^{2+}]_{cyt}$ based on the simulations for $InsP_3$ and $GPIP_2$ stimulation (at the same concentrations measured in the experiments). The rate for metabolite degradation was determined for the two conditions to optimize the fit to each set of averaged experimental points; the resultant time constants were 0.8 s for $InsP_3$ and 13 s for $GPIP_2$. For comparison, degradation curves for $InsP_3$ are also included as dotted curves. (*b*) The model can also be used to simulate a dose response series for the calcium response to varying levels of uncaged $InsP_3$ in a single cell. The cell used for Fig. 3 is shown again here (*open circles*); simulation results are shown as a solid line. (*c*) Using the same parameters as for the dose-response in (*b*), we simulated the full time course for four concentrations of uncaged $InsP_3$. Experimental data are shown as light curves and simulation results as heavy curves.

particular cell, the best fit is found at $\tau = 1.3$ s, as opposed to 0.8 s found for the average data in Fig. 4 *a*. The lag before the onset of the response, the maximum amplitude of the response, and the decay of the response are all fit nicely by the model for levels of uncaging corresponding to just above threshold, close to half maximal, and close to maximal stimulation of Ca release. It should be emphasized that many of the parameters in Table 1 are either specified or highly constrained by our experiments and data from the literature. The fact that the data in all three parts of Fig. 4 display good correspondence between experiment and simulation supports the adequacy of the model for our purposes.

DISCUSSION

In this paper, we have measured the $[InsP_3]_{cyt}$ required to evoke calcium release in A7r5 cells. By fitting the Hill equation to individual cell data for the calcium response to increasing concentrations of uncaged $InsP_3$, values for EC_{50} and Hill coefficient could be determined for the A7r5 cells. We obtained an EC_{50} for half-maximal $InsP_3$-mediated calcium release of approximately 100 nM. This value agrees quite well with previous estimates of $InsP_3$ necessary for calcium release in these cells using alternate methods (Missiaen et al., 1996; Sienaert et al., 1997). The molecular basis for the Hill coefficient of 2.5 is most likely the requirement for the binding of multiple $InsP_3$ molecules to initiate channel opening. Our value for the Hill coefficient is in agreement with values obtained for the Type 1 $InsP_3$ receptor in other cell types, using reconstituted channels in lipid bilayers (Bezprozvanny et al., 1991a) and quantitative uncaging (Oancea and Meyer, 1996). However, it should be noted that the primary purpose of using the Hill equation to fit the data was to compare our results to those of others and to compare

the behavior of $InsP_3$ and $GPIP_2$. The Hill equation should be considered phenomenological and does not formally represent a mechanistic model. We have been able to model the behavior of the system via a combination of models for the $InsP_3$ receptor (De Young and Keizer, 1992; Li and Rinzel, 1994), SERCA pumps (Lytton et al., 1992; Sneyd et al., 1995), and calcium buffers (Wagner and Keizer, 1994).

Our method for calibrating $[InsP_3]_{cyt}$ after uncaging is an adaptation of previous uncaging experiments, and we used these calibrations to obtain dose response curves for $InsP_3$-mediated calcium release. Previous methods for determining uncaging efficiency have involved solutions in either a cuvette or a micropipette. Here, we wished to calibrate the efficiency of uncaging with an optical path similar to that employed for cells. We used a cell-sized aqueous droplet of solution on a coverslip and assayed uncaging efficiency as a function of pH change measured with a fluorescent pH indicator. The assumption that caged ATP will uncage with the same efficiency as caged $InsP_3$ (Walker et al., 1989) was validated with a limited number of calibrations with caged $InsP_3$, directly measuring the concentration released by uv light by means of a competitive radioligand binding assay. The relationship obtained for uncaging efficiency versus light dosage was linear and intersected at the origin, strengthening the validity of our methods. Another internal validation was that similar $InsP_3$ sensitivities were measured from two microscope setups, each individually calibrated.

In addition to uncaging efficiency, it was important to know the concentration of caged $InsP_3$ in the cell to accurately determine uncaged $[InsP_3]_{cyt}$. With whole cell patch experiments, this is not a concern, as the pipette solution equilibrates with the cytosol. However, this could seriously disrupt the intracellular milieu and not properly reflect the $InsP_3$-mediated calcium release in a fully intact cell. We have developed a method for accurately determining intracellular fluorescent probe concentrations by confocal microscopy (Fink et al., 1998) and applied these methods to calculating concentrations here. In this particular case, the fluorescence of a coinjected indicator dye measured in the middle of the soma was imaged with confocal microscopy; based on convolution of a solid model with the confocal point spread function, this region of the cell is known to be unaffected by intensity blurring (Fink et al., 1998). This measurement is not only convenient, but also provides the intracellular concentration of exogenous Ca^{2+} buffer (i.e., Calcium Green-1 dextran) needed as input to the modeling. Our calculations are accurate as long as the caged $InsP_3$ and the dye are distributed uniformly throughout the cell. Another source of error would be from altered calcium levels in the injected cells; this would give a brighter Calcium Green signal and cause us to overestimate the concentration of $InsP_3$ uncaged. Checking our measurement techniques with controls of injected Calcium Green and Texas Red-dextran showed that we had made a reasonable estimate of the resting level of calcium in these cells. If a particular cell has an unusually high resting level of calcium (and Calcium Green fluorescence), the cell is most likely damaged and would fail to produce a good dose response to increasing concentrations of uncaged $InsP_3$.

Degradation rates for $InsP_3$ and calcium extrusion efficiencies can be calculated by analyzing $[Ca^{2+}]_{cyt}$ recovery after stimulus with a pulse of $InsP_3$ or $GPIP_2$, a slowly metabolized analogue of $InsP_3$. The effectiveness of $GPIP_2$ to initiate calcium release was several times lower than that of $InsP_3$, which is in agreement with previous findings (Bird et al., 1992). Some events crucial to the $[Ca^{2+}]_{cyt}$ recovery mechanisms are not dependent on a decline in $InsP_3$ concentration; these include, among others, $InsP_3$ channel inhibition, calcium store refilling, calcium extrusion across the plasma membrane, and calcium uptake by mitochondria. It is possible that these processes might dominate the recovery of $[Ca^{2+}]_{cyt}$ to baseline levels if they are sufficiently active or up-regulated during the signaling process. However, the fact that there is a difference in the $[Ca^{2+}]_{cyt}$ relaxation for the two metabolites suggests that $InsP_3$ degradation is required before $[Ca^{2+}]_{cyt}$ can recover to baseline levels. Thus, in these cells, the negative feedback associated with Ca^{2+} binding to the inhibitory site on the $InsP_3$ receptor channel is insufficient, by itself, to close the channel as long as $InsP_3$ remains high.

Using the Virtual Cell, an interactive model construction program (Schaff et al., 1997), we were able to derive parameters that could fit the time courses of $[Ca^{2+}]_{cyt}$ relaxation back to baseline following stimulation of Ca release by uncaging either $InsP_3$ or $GPIP_2$. The data are consistent with a time constant of 0.8 s for the degradation of $InsP_3$ in the cell, similar to previous estimates in other cell types (Wang et al., 1995; Burgess et al., 1985); in particular, the time constant of $InsP_3$ has been measured to be $\sim$1 s in smooth muscle cells from the rabbit main pulmonary artery (Walker et al., 1987). In addition, we determined a 13-s time constant for the degradation of $GPIP_2$. It should also be noted that the parameter set (Table 1) was highly constrained by the experimental values derived in this study and taken from the literature.

The validity of the model is further supported by its ability to fit the dose-response relationship of $[Ca^{2+}]$ release to $[InsP_3]_{cyt}$ in a typical single cell and to fit the complete time course for the calcium response to various levels of uncaged $InsP_3$ in the same cell (Fig. 4, *b* and *c*). Clearly, not all the individual components of the calcium handling machinery of the cell were explicitly included, but are probably included implicitly in the parameters of components with similar functions. For example, uptake by mitochondria may be subsumed within the generalized endogenous buffers and the plasma membrane Ca pump may be implicitly covered by the SERCA activity. The mechanism for the Type 1 $InsP_3R$ in our model is based on an analysis (De Young and Keizer, 1992; Li and Rinzel, 1994) of the single channel recordings obtained for this receptor reconstituted in planar lipid bilayers (Bezprozvanny et al., 1991). Other models for the Type 1 $InsP_3R$ have been proposed, including a significant reformulation based on patch clamp data from the nuclear membrane of *Xenopus* oocytes (Mak et al.,

1998). We have not attempted to determine in detail how well our data might be accommodated by these alternative mechanisms for the $InsP_3R$. However, a qualitative consideration of the mode of $InsP_3$ R channel gating proposed by Mak et al. (1998) indicates that several parameters associated with other components of the overall model would have to be significantly altered, including the degradation time for $InsP_3$.

It is instructive to consider the sensitivity analysis in Table 2 in order to better appreciate the key factors that control the shape of the calcium curve. It is important to understand that these sensitivities are dimensionless quantities representing the relative change in calcium divided by a small relative change in the parameter. This is, therefore, equivalent to $\partial\log[Ca^{2+}]_{cyt}/\partial\log\alpha$. The times tabulated in Table 2 correspond to the end of the lag time between the uncaging event and the start of the calcium rise (0.25 s), the peak amplitude of the calcium transient (0.75 s), and a point during the calcium recovery phase (7.0 s). The initiation of the calcium rise is most strongly controlled by the dissociation constant of the activating calcium binding site on the $InsP_3$ receptor (K_{act}) and the calcium flux through the channel (J_{max}); thus, positive feedback by calcium is a primary determinant of the lag time before the start of the calcium signal. These two parameters are also important for the maximum amplitude of the $[Ca^{2+}]_{cyt}$ rise, but, interestingly, the rate for binding of calcium to the inhibitory site (K_{inh}, k_{on}) now exerts an important negative influence at t = 0.75 s. Calcium binding to the inhibitory site remains an important factor during the recovery period, when the turnover of the SERCA pump (K_p, V_{max}) becomes the dominant component. Interestingly, the parameters associated with $InsP_3$ binding to its receptor ($[I]_0$, $[I]_{unc}$, and K_I), have a uniform influence on the calcium signal throughout the time course. Although this sensitivity is moderate, its constancy helps to explain the prerequisite for $InsP_3$ degradation before the $[Ca^{2+}]_{cyt}$ can return to baseline levels. It should also be noted that Table 2 refers to an experiment with 0.858 μM uncaged $InsP_3$ (corresponding to Fig. 4 *a*). At lower levels of $InsP_3$, the sensitivity to $[I]_0$, $[I]_{unc}$, and K_I all would increase. Finally, sensitivity to τ becomes significant only for the $[Ca^{2+}]_{cyt}$ recovery phase. This is satisfyingly consistent with our conclusions from the experimental difference between $InsP_3$ and $GPIP_2$ uncaging. This analysis, thus, provides insights into how the various factors governing individual molecular events can alternately come into play to control the features of the calcium signal.

In conclusion, we demonstrated a method for quantitative measurement of $InsP_3$ uncaging in microinjected A7r5 cells. This method can be used to determine the amount of $InsP_3$ required in intact cells to initiate calcium release. A full model for the time course of $InsP_3$-dependent $[Ca^{2+}]_{cyt}$ changes in this cell can be constructed from a model of the $InsP_3$ receptor together with considerations of calcium buffering in the cytosol and calcium reuptake into the ER via SERCA pumps; plasma membrane influx or efflux need not be included, at least for uncaged $InsP_3$. A pair of important values were derived from our combined experimental and modeling analysis: the concentration of $InsP_3$ required for 50% activation of calcium release from the ER in these smooth muscle cells is ~100 nM; the intracellular degradation rate of $InsP_3$ has a time constant of 0.8 s. Although the overall process is only moderately sensitive to $InsP_3$, $InsP_3$ degradation is a prerequisite for calcium recovery to prestimulus levels. Furthermore, the 8-state model of DeYoung and Keizer (1992) is sufficient to describe the behavior of the type I $InsP_3$ receptor in these cells. The approaches we have developed and the insights gained for the A7r5 cells should form a good basis for detailed studies of $InsP_3$-mediated calcium signals initiated by physiological stimuli.

We thank Ion Moraru and Jim Watras for many helpful discussions. Yale Goldman supplied the caged ATP. Jim Schaff developed the Virtual Cell system and provided much advice on the construction and analysis of the model. The staff of the Center for Biomedical Imaging Technology offered invaluable help in the acquisition and analysis of the microscopy data. We are pleased to acknowledge support from the National Institutes of Health through grants RR13186 and GM35063.

REFERENCES

Benevolensky, D., I. Moraris, J. Watras. 1994. Micromolar calcium reduces the affinity of the inositol 1,4,5-triphosphate receptor in smooth muscle. *Biochem. J.* 299:631–636.

Berridge, M. J. 1993. Inositol trisphosphate and calcium signalling. *Nature.* 361:315–325.

Bezprozvanny, I., J. Watras, and B. E. Ehrlich. 1991. Bell-shaped calcium-response curves of Ins(1, 4, 5)P_3-and calcium-gated channels from endoplasmic reticulum of cerebellum. *Nature.* 351:751–754.

Bird, G. J., J. F. Obie, and J. W. J. Putney. 1992. Sustained Ca2+ signaling in mouse lacrimal acinar cells due to photolysis of "caged" glycerophoshphoryl-myo-inositol 4,5-bisphosphate. *J. Biol. Chem.* 267: 17722–17725.

Blatter, L. A., and W. G. Wier. 1992. Agonist-induced $[Ca^{2+}]_i$ waves and Ca2+-induced Ca2+ release in mammalian vascular smooth muscle cells. *Am. J. Physiol.* 263:H576–H586.

Burgess, G. M., J. S. McKinney, R. F. Irvine, and J. W. Putney. 1985. Inositol 1,4,5-triphosphate and inositol 1,3,4-triphosphate formation in Ca2+-mobilizing-hormone-activated cells. *Biochem. J.* 232:237–243.

De Smedt, H., L. Missiaen, J. B. Parys, R. H. Henning, I. Sienaert, S. Vanlingen, A. Gijsens, B. Himpens, and R. Casteels. 1997. Isoform diversity of the inositol triphosphate receptor in cell types of mouse origin. *Biochem. J.* 322:575–583.

De Young, G. W., and J. Keizer. 1992. A single-pool inositol 1,4,5-trisphosphate-receptor-based model for agonist-stimulated oscillations in Ca2+ concentration. *Proc. Natl. Acad. Sci. USA.* 89:9895–9899.

Dupont, G., and C. Erneux. 1997. Simulations of the effects of inositol 1,4,5-trisphosphate 3-kinase and 5-phosphatase activities on Ca2+ oscillations. *Cell Calcium.* 22:321–331.

Eberhard, M., and P. Erne. 1991. Calcium binding to fluorescent calcium indicators: calcium green, calcium orange, and calcium crimson. *Biochem. Biophys. Res. Comm.* 180:209–215.

Fink, C., F. Morgan, and L. M. Loew. 1998. Intracellular fluorescent probe concentrations by confocal microscopy. *Biophys. J.* 75:1648–1658.

Gill, D., and S.-H. Chueh. 1985. An intracellular (ATP + Mg2+)-dependent calcium pump within the N1E-115 neuronal cell line. *J. Biol. Chem.* 260:9289–9297.

Glanville, N., D. Byers, H. Cook, M. Spence, and F. Palmer. 1989. Differences in the metabolism of inositol and phosphoinositides by cultured cells of neuronal and glial origin. *Biochem. Biophys. Acta.* 1004:169–179.

Grynkiewicz, G., M. Poenie, and R. Y. Tsien. 1985. A new generation of Ca^{2+} indicators with greatly improved fluorescence properties. *J. Biol. Chem.* 260:3440–3450.

Hagar, R. E., and B. E. Ehrlich. 1998. Comparison of the single channel properties of the type I and type III InsP3 receptors. *Biophys. J.* 74: A323. (abstr.)

Hall, J. 1992. Bradykinin receptors: pharmacological properties and biological roles. *Pharmacol. Ther.* 56:131–190.

Khodakhah, K., and D. Ogden. 1993. Functional heterogeneity of calcium release by inositol trisphosphate in single Purkinje neurones, cultured cerebellar astrocytes, and peripheral tissues. *Proc. Natl. Acad. Sci. USA.* 90:4976–4980.

Khodakhah, K., and D. Ogden. 1995. Fast activation and inactivation of inositol triphosphate-evoked Ca2+ release in rat cerebellar Purkinje neurones. *J. Physiol.* 487.2:343–358.

Kimes, B. W., and B. L. Brandt. 1976. Characterization of two putative smooth muscle cell lines from rat thoracic aorta. *Exp. Cell Res.* 98: 349–366.

Kupferman, R., P. P. Mitra, P. C. Hohenberg, and S. S.-H. Wang. 1997. Analytical calculation of calcium wave characteristics. *Biophys. J.* 72: 2430–2444.

Li, Y. X., and J. Rinzel. 1994. Equations for InsP3 receptor-mediated $[Ca^{2+}]_i$ oscillations derived from a detailed kinetic model: a Hodgkin-Huxley like formalism. *J. Theor. Biol.* 166:461–473.

Luzzi, V., H. A. Fishman, C. E. Sims, and N. L. Allbritton. 1996. A novel strategy for measurement of inositol 1,4,5-triphosphate (IP3) concentrations in single Xenopus oocytes. *Mol. Biol. Cell.* 7S:370a.

Lytton, J., M. Westlin, S. E. Burk, G. E. Shull, and D. H. MacLennan. 1992. Functional comparisons between isoforms of the sarcoplasmic or endoplasmic reticulum family of calcium pumps. turnover rate for SERCA2b, the ubiquitous isoform, is ca 3/s. also give data on Ca and ATP dependences. *J. Biol. Chem.* 267:14483–14489.

Mak, D. O. D., S. McBride, and J. K. Foskett. 1998. Inositol 1,4,5-trisphosphate activation of inositol tris-phosphate receptor Ca2+ channel by ligand tuning of Ca2+ inhibition. *Proc. Natl. Acad. Sci. USA.* 95:15821–15825.

Meldolesi, J., and T. Pozzan. 1998. The endoplasmic reticulum Ca2+ store: a view from the lumen. *Trends Biochem. Sci.* 23:10–14.

Missiaen, L., H. De Smedt, G. Droogmans, and R. Casteels. 1992. Ca2+ release induced by inositol 1,4,5-triphosphate is a steady-state phenomenon controlled by luminal Ca2+ in permeabilized cells. *Science.* 357: 599–602.

Missiaen, L., J. B. Parys, H. De Smedt, F. X. Lemaire, I. Sienaert, M. D. Bootman, and R. Casteels. 1995. Slow kinetics of InsP3-induced Ca2+ release: differences between uni- and bi-directional 45Ca2+ fluxes. *Cell Calcium.* 18:100–110.

Missiaen, L., H. De Smedt, J. B. Parys, I. Sienaert, S. Vanlingen, and R. Casteels. 1996. Threshold for inositol 1,4,5-triphosphate action. *J. Biol. Chem.* 271:12287–12293.

Missiaen, L., H. De Smedt, J. B. Parys, I. Sienaert, H. Sipma, S. Vanlingen, and R. Casteels. 1997. Slow kinetics of inositol 1,4,5-triphosphate-induced Ca2+ release: is the release 'quantal' or 'non-quantal'? *Biochem. J.* 323:123–130.

Miyawaki, A., J. Llopis, R. Heim, J. M. McCaffery, J. A. Adams, M. Ikura, and R. Y. Tsien. 1997. Fluorescent indicators for Ca2+ based on green fluorescent proteins and calmodulin [see comments]. *Nature.* 388: 882–887.

Oancea, E., and T. Meyer. 1996. Reversible desensitization of inositol triphosphate-induced calcium release provides a mechanism for repetitive calcium spikes. *J. Biol. Chem.* 271:17253–17260.

Ogden, D., and T. Capiod. 1997. Regulation of Ca2+ release by InsP3 in single guinea pig hepatocytes and rat Purkinje neurons. *J. Gen. Physiol.* 109:741–756.

Ramos-Franco, J., M. Fill, and G. A. Mignery. 1998a. Isoform-specific function of single inositol 1,4,5-trisphosphate receptor channels. *Biophys. J.* 75:834–839.

Ramos-Franco, J., P. Perez, S. Caenepeel, G. Mignery, and M. Fill. 1998b. Distinct calcium regulation patterns of type-1 and type-2 inositol 1,4,5-triphosphate receptors. *Biophys. J.* 74:A61.

Regoli, D., F. Gobeil, Q. Nguyen, D. Jukic, P. Seoane, J. Salvino, and D. Sawutz. 1994. Bradykinin receptor types and B2 subtypes. *Life Sci.* 55:735–749.

Schaff, J., C. C. Fink, B. Slepchenko, J. H. Carson, and L. M. Loew. 1997. A general computational framework for modeling cellular structure and function. *Biophys. J.* 73:1135–1146.

Sienaert, I., L. Missiaen, H. De Smedt, J. B. Parys, H. Sipma, and R. Casteels. 1997. Molecular and functional evidence for multiple Ca2+-binding domains in the type 1 inositol 1,4,5-triphosphate receptor. *J. Biol. Chem.* 272:25899–25906.

Sims, C. E., and N. L. Allbritton. 1998. Metabolism of inositol 1,4,5-triphosphate and inositol 1,3,4,5-tetrakiphosphate by the oocytes of *Xenopus laevis*. *J. Biol. Chem.* 273:4052–4058.

Sneyd, J., J. Keizer, and M. J. Sanderson. 1995. Mechanisms of calcium oscillations and waves: a quantitative analysis. *FASEB J.* 9:1463–1472.

Sugiyama, T., and W. F. Goldman. 1995. Conversion between permeability states of IP3 receptors in cultured smooth muscle cells. *Am. J. Physiol.* 269:C813–C818.

Wagner, J., and J. Keizer. 1994. Effects of rapid buffers on Ca2+ diffusion and Ca2+ oscillations. *Biophys. J.* 67:447–456.

Walker, J. W., A. V. Somlyo, Y. E. Goldman, A. P. Somlyo, and D. R. Trentham. 1987. Kinetics of smooth and skeletal muscle activation by laser pulse photolysis of caged inositol 1,4,5-triphosphate. *Nature.* 327: 249–252.

Walker, J. W., G. P. Reid, J. A. McCray, and D. R. Trentham. 1988. Photolabile 1-(2-nitrophenyl)ethyl phosphate esters of adenine nucleotide analogues: synthesis and mechanism of photolysis. *J. Am. Chem. Soc.* 110:7170–7177.

Walker, J. W., J. Feeney, and D. R. Trentham. 1989. Photolabile precursers of inositol phosphates. preparation and properties of 1-(2-nitrophenyl-)ethyl esters of myo-inositol 1,4,5-triphosphate. *Biochemistry.* 28: 3272–3280.

Wang, S. S.-H., A. A. Alousi, and S. H. Thompson. 1995. The lifetime of inositol 1,4,5-trisphosphate in single cells. *J. Gen. Physiol.* 105: 149–171.

Watras, J., and D. Benevolensky. 1987. Inositol 1,4,5-trisphosphate induced calcium release from canine aortic sarcoplasmic reticulum vesicles. *Biochim. Biophys. Acta.* 731:354–363.

Wojcikiewicz, R. J. H. 1995. Type I, II, and III inositol 1,4,5-triphosphate receptors are unequally susceptible to down-regulation and are expressed in markedly different proportions in different cell types. *J. Biol. Chem.* 270:11678–11683.

Wootton, J. F., J. E. T. Corrie, T. Capiod, J. Feeney, D. R. Trentham, and D. C. Ogden. 1995. Kinetics of cytosolic Ca2+ concentration after photolytic release of 1-D-myo-inositol 1,4-bisphosphate 5-phosphorothioate from a caged derivative in guinea pig hepatocytes. *Biophys. J.* 68:2601–2607.

Xu, T., M. Naraghi, H. Kang, and E. Neher. 1997. Kinetic studies of Ca2+ binding and Ca2+ clearance in the cytosol of adrenal chromaffin cells. *Biophys. J.* 73:532–545.